Design of a low velocity wind turbine blades for power generation: part I-aerodynamic performance

B G SUHAS[1,*] , B K SREEJITH[2], A R ANIL CHANDRA[1], SHIVASHANKAR R SRIVATSA[1] and V PREMA[3]

[1]Department of Mechanical Engineering, B.M.S College of Engineering, Bull Temple Road, Bengaluru, Karnataka 560019, India
[2]Department of Mechanical Engineering, A J Institute of Engineering and Technology Mangalore, Dakshina Kannada, Karnataka 575013, India
[3]Department of Electrical and Electronics Engineering, B.M.S College of Engineering, Bull Temple Road, Bengaluru, Karnataka 560019, India
e-mail: suhas_bg@yahoo.co.in

Abstract. Harnessing energy from low wind velocity requires the design of small-scale wind turbines using airfoils that can operate at a low Reynolds number ($Re < 500,000$). However, at low Re, the aerodynamic performance of the blade is reduced due to bubble drag along with viscous friction and pressure drag. The objective of present work is to design and analyze the horizontal axis wind turbine blade to meet the power coefficient at optimized tip speed ratio. Based on the annual average wind speed at the location of installation, the design wind speed was calculated to be ~ 7.25 m/s at a hub height of 10 m according to the IEC standard. A 1.1 m long blade consisting of Wortmann FX 63-137 airfoil was designed using blade element momentum (BEM) theory. The blade design was optimized to achieve better performance for a wide range of tip speed ratios (λ) by the combination method. The performance curves for the optimized blade design were obtained analytically using MATLAB® programs based on BEM theory. Using multiple reference frame Moving Reference Frame approach, computational fluid dynamics (CFD) simulation was performed in ANSYS Fluent® to determine the performance of the turbine in terms of power coefficient (C_p) under complex three-dimensional fluid flow. The CFD simulation methodology was validated using the experimental data available in the literature.

Keywords. Low wind speed turbine; laminar separation bubble; FX 63-137 airfoil; BEM theory; power coefficient.

1. Introduction

The worldwide energy demand has been on the rise due to the rapidly increasing population and industrial growth. Countries are meticulously planning and investing in renewable energy production to meet the increasing energy requirements and at the same time reduce the dependency on conventional energy sources. Due to the challenges involved in the transmission of power from a major centralized power grid to distant locations, there are several remote areas in developing countries that are deprived of electricity. A feasible solution for electrification of such remote and isolated localities is a microgrid. The current project funded by Dassault system is to explore the possibility of harnessing wind energy for the upliftment of tribals

located in such remote areas. In this regard Manchenahalli village of Chikkaballapura district in the outskirts of Bengaluru city was selected for the execution of the project. To meet the interconnected load requirements for microgrid, horizontal axis wind turbine (HAWT) and vertical axis wind turbines (VAWT) may be installed [1, 2]. These are the two major types of wind turbines classified based on the orientation of the axis of rotation of the turbine rotor. In the rural areas where predominantly low wind speeds are observed, electrification using microgrid technology with small wind turbines are a suitable solution when compared to large wind turbines. According to the IEC Standard for small wind turbine safety, IEC 61400-2, wind turbines having a swept area of fewer than 200 m^2 are categorized as small wind turbines. Both small and large wind turbines operate on the same principle i.e., the turbine blade is made of several airfoil sections throughout its span and the

*For correspondence

aerodynamic forces generated by these airfoil sections cause the rotation of the blade. However, small turbines differ from large turbines in few aspects. The category of small wind turbines is dominated by HAWT [3, 4]. This is because HAWTs are more efficient and require lesser installation and maintenance costs when compared to VAWTs. Blade element momentum (BEM) theory is the most widely used theory to determine the aerodynamically efficient blade shape and to calculate the performance of the designed rotor. According to this theory, the blade is divided into several sections along the blade span. The chord length and section pitch angle for each blade section are then determined using the lift and drag characteristics of the selected airfoil for the design angle of attack. Krishnanunni *et al* [5] used the BEM theory was to design a 3.4 m long blade intended to produce a rated power of 250 W at 4.2 ms^{-1}. The chord distribution obtained from BEM theory was modified by drawing a straight line through 70% and 90% span (length of the blade) in order to reduce the material near the root. This linearization technique is an approach to simplify the chord length distribution during blade design. However, such linearization attempts have seldom been attempted with combination of chord length and section pitch angle distribution. Muhsen *et al* [6] employed BEM theory to design the blade for a 4 m diameter rotor using an airfoil interpolated between the S1210 and S1223 airfoils. The power coefficient (C_p) of the designed blade was calculated using MATLAB® code. The design was optimized to obtain higher than 40% at a low wind speed of 5 ms^{-1} using the Qblade® software. Singh and Ahmed [7] designed a 1.26 m diameter rotor with 2 twisted and tapered blades. This was named as AF300 and was designed using BEM theory. The designed blades yielded a better power coefficient of 0.29 when compared with that of baseline Air-X wind turbine having power coefficient value of 0.2. Song and David [8] used BEM theory to design and fabricate the blades of a 2.5 m diameter rotor to produce a rated power of 1 kW at a wind speed of 11 ms^{-1}. The designed blades were fit to the Bergey XL 1.0 wind turbine and subjected to field tests using the vehicle-based platform. It was observed that the difference in rotor performance using BEM theory had predicted well in comparison with the test results. Similar work by Refan *et al* [9] on the applicability of BEM theory for predicting the performance of 2.2 m diameter HAWTs showed good results. Wood [10] developed a MATLAB® program based on BEM theory to determine the performance of a wind turbine at different wind speeds and tip speed ratios. The power and thrust coefficients predicted using the MATLAB® code were found to be within 10% of the experimental measurements. The blades of a small turbine typically operate at a Reynolds number (R_e) less than 500,000 which is much lesser than the operational for a large turbine blade [11]. Also, the blades of a small turbine experience greater centrifugal load when compared to

the large turbine blades because of their higher rotational speeds [12]. Remote localities lying in low wind speed regions that need to be electrified would be operating at Reynolds number below the operational range for a large turbine. In such circumstances, small turbines with good low wind performance can efficiently extract the energy available in wind. Power generated by the wind turbine is directly proportional to implying, greater the value of better is the design of the blade [13]. However, maximizing should not be the only objective while designing the blade. It is always desirable to design a blade that has better over a wide range of tip-speed ratio (λ) [14]. Moreover, BEM theory has shown limited success in cases where Re is very low of 50,000 The linearized rotor has lesser performance than its BEMT counterpart but could potentially serve as an off-grid power source [15]. Therefore, in the present work Blade Design by Linearization of chord distribution and section pitch angle is attempted and is the novelty of the work.

The initial blade design obtained using the BEM theory exhibits suitable performance close to optimized tip-speed ratio (λ_{opt}). Such approach will have a non-linear distribution of chord length and section pitch angle which makes it difficult from the manufacturing point of view. Adopting the linearized one would be suitable for operation not only in windy areas but also in low wind speed regions [16]. Therefore, the initial blade shape obtained from BEM theory is usually optimized by linearizing the chord and section pitch angle distribution [17]. For ease of fabrication, Burton proposed linearization of chord length by drawing a straight line through the chord lengths at 90% and 70% blade spans of the initial shape [18]. However, Wood [19] showed that the hubregion is pivotal for better starting performance, and the linearization of the chord that causes a reduction in the width of the initial blade shape is not preferred for small speed turbine blades. Therefore, a novel attempt is made to arrive at the blade shape by different combinations of chord length and section pitch angle distribution in the process of linearization. The combination is subsequently explained in detail in section 3.2.

The objectives of the present work are as follows:

- Design of a wind turbine blade using combination method to operate at low wind speeds.
- Optimization of the blade design for enhancing the power coefficient over a range of tip speed ratios.
- Carrying out 3D CFD simulation of the flow over the optimized wind turbine rotor to determine the wind energy captured by the rotor and comparison of the same with the results of BEM theory.

Overall, the present work highlights the effective use of numerical tools in design and optimization of the wind turbine blade for low wind velocity applications, specifically the linearization with combination of chord length and section pitch angle distribution.

2. Methodology

The methodology followed in the present work is shown in figure 1. The annual average wind speed at the location of installation is used to determine the size of the wind turbine blade required to generate the necessary power. From the preliminary analysis of airfoils that are suitable for low applications, a suitable airfoil is selected for the blade profile. The BEM theory, a 2D approach, is used to determine the initial shape of the blade and calculate its performance analytically. The initial blade shape is optimized by linearizing the chord and twist angle distribution, a novel approach, to obtain wider performance curves at different operational wind speeds by combination method.

Analytically determined performance curves are used to choose the optimum blade design. Steady-state CFD simulation is then carried out to determine the power generated by the optimized rotor under complex 3D flow. The CFD simulation procedure is then validated against the experimental data available in the literature. The theory divides the blade into several elements and the forces acting on

each element are determined by considering two-dimensional flow over it. The total force acting on the blade is then obtained by integrating the forcesacting on these elements. Though the theory is well-established, it tends to over predict the performance of the turbines due to its assumptions and simplifications [20, 21]. Besides, BEM theory uses the lift and drag data of the airfoils to predict the performance of the blade. Hence, the accuracy of the prediction depends on the accuracy of the data available for the airfoil. Therefore, three-dimensional computational fluid dynamics (CFD) simulation is carried out to determine the performance of the optimized blade at different wind speeds ranging from 5 to 10 ms^{-1}.

Steady-state simulations were performed on this blade using the MRF approach in ANSYS® Fluent software. MRF approach approximates the actual flow phenomenon to a steady-state problem where an inner rotating domain encloses the turbine rotor and an outer stationary domain to which the boundary conditions are applied. The angular velocity of the rotor is applied to the inner domain. However, the inner domain does not rotate during simulation. Only the flow parameters in the inner domain are solved
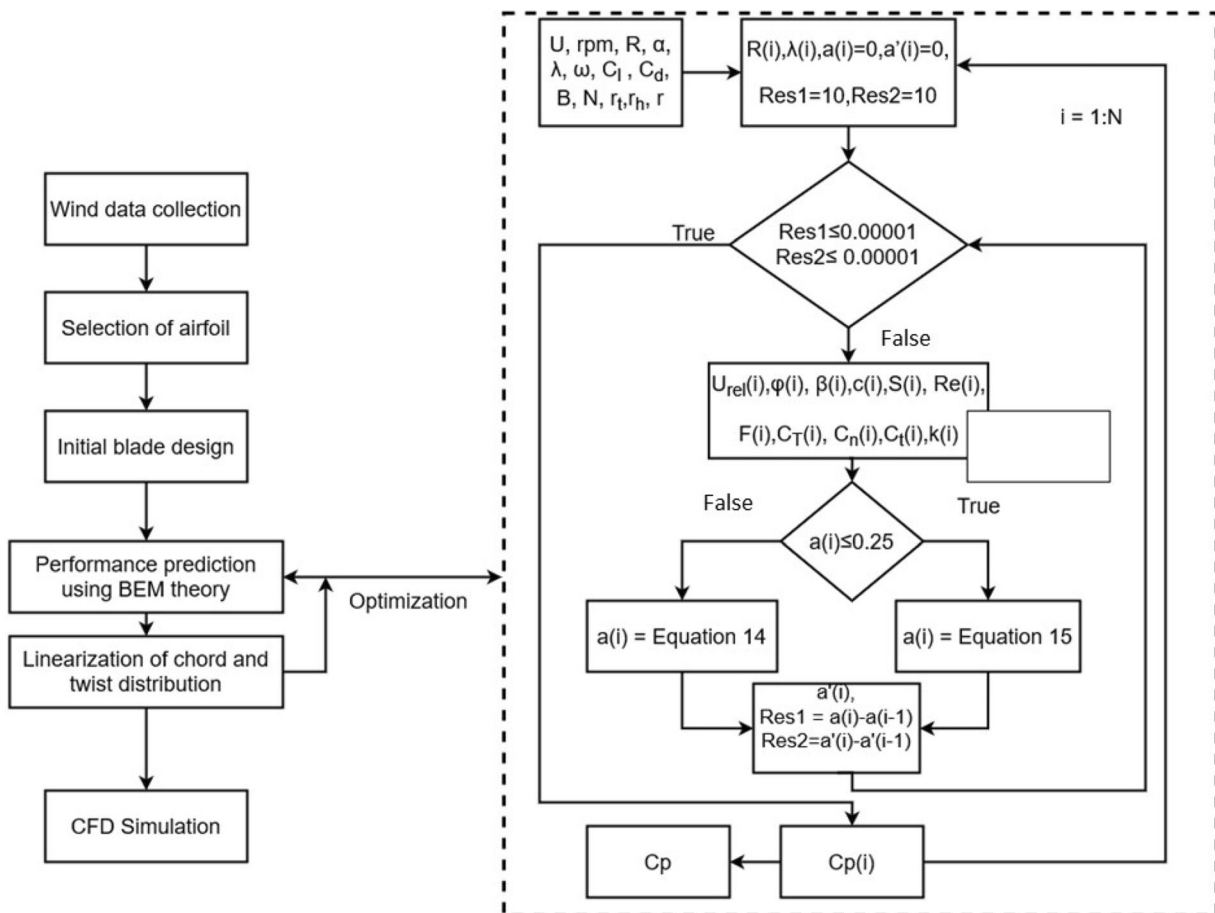

Figure 1. Wind turbine blade design procedure.

using MRF equations. Generally, the outer domain is modelled large enough to avoid the boundary effects. The geometry of the computational domains used in the present work is shown in figure 2(a). The dimensions of the domains are shown in figure 2(b).

The domain is created in ANSYS software with dimensions as shown in figure 2(b) where sufficiently long downwind flow side is maintained to capture the wake. An unstructured mesh consisting of tetrahedral elements was generated using ANSYS Mesh®. The outer stationary domain has a diameter of 13 m and a total length of 17 m is provided and sufficiently long down-wind flow side is maintained to capture the wake. An unstructured mesh consisting of tetrahedral elements was generated using ANSYS Mesh®. The inner rotating domain has a diameter of 2.5 m and length of 0.5 m which sufficient just cover the turbine is provided with fine mesh. Face sizing was applied on the interfaces between the domains and the Contact match option was used to generate identical mesh for the interfaces between the two domains. This ensures better flow continuity between the two domains even though the outer domain has a relatively coarser mesh. Matching interface option is selected for the interfaces between the two domains so that the wall zones are not created on the interfaces. The boundary conditions applied are also shown in figure 2(a). Velocity-inlet and pressure-outlet boundary conditions are applied to the inlet and outlet respectively. 'Free slip wall' condition is applied to the circumference of the outer domain. The angular velocity (Ω) to be applied to the inner domain for a particular wind speed and is determined using Equation 15. The turbulence model includes in the SST turbulence model [22], which were solved in a Moving Reference Frame (MRF) that attached to the blades with the assumptions of incompressible and steady-state turbulent flow. All computations are performed assuming the fully turbulent flow, excluding the transitional effects in the region of the blade. This turbulence model was used for

the simulation because of its suitability for boundary layer flow as well as freestream flow. A mesh consisting of 924,922 elements was selected for simulation based on the grid independence study. Figure 3(a), shows the rotating domain with fine mesh and the stationary domain containing a relatively coarser mesh. The surface mesh that accurately captures the surface of the blade is also shown in figure 3(b).

The free stream temperature used to calculate the fluid characteristics is 300 K, the same as the environment temperature. Air is selected as the fluid material having density of 1.225 (kg/m^3) and dynamic viscosity of $1.7894 * 10^{-5}$ (kg/ms). The flow turbulence level is set to 5% and treated as incompressible. The solution method is chosen as coupled, which is a robust and efficient single-phase implementation for steady-state flows and second order upwind spatial discretization are applied during the simulation. Spatial gradient is fixed to the least square cell method. The convergence criteria are fixed at a residual target of 10^{-5}. The simulation is carried out for inlet velocity of 5.5 m/s and TSR of 6.5. Current study focuses only on the pressure distribution over the blade and hence the C_p generation of the turbine. In that perception, as many researchers followed RANS SST $k - \omega$ turbulence model for the purpose [23], same approach is followed in the present study.

3. Results and discussions

3.1 *Wind data collection*

The first step towards designing the wind turbine blade is to assess the wind data at the location of installation. Figure 4 shows the Weibull probability distribution of wind speed at the installation site generated by the WASP® software. The wind data to generate the Weibull distribution was
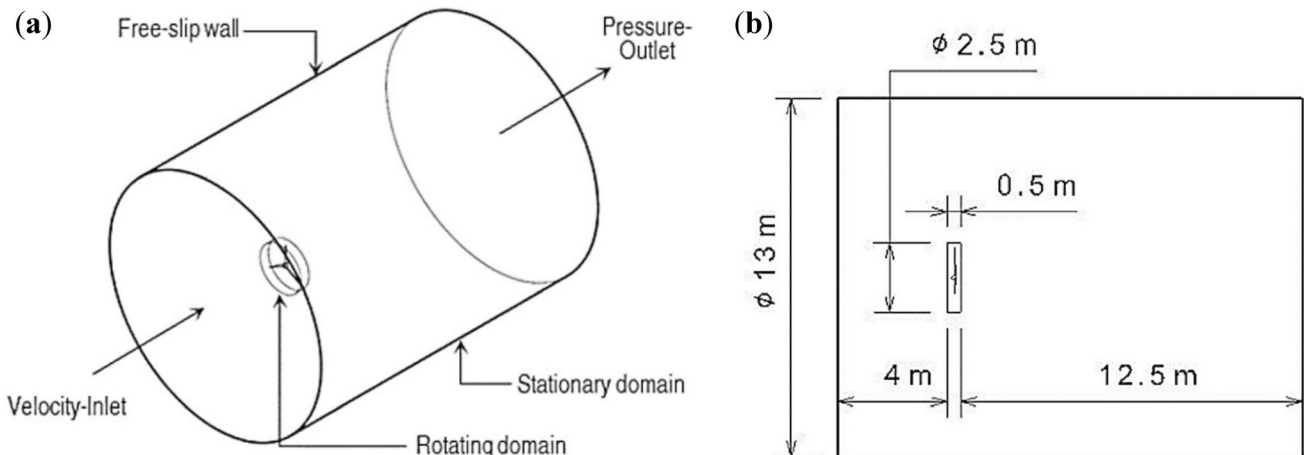
Figure 2. (**a**) Geometry of the computational domains along with the boundary conditions. (**b**) Dimensions of the inner and outer domains.

(a)　　　　　　　　　　　　　　　　**(b)**
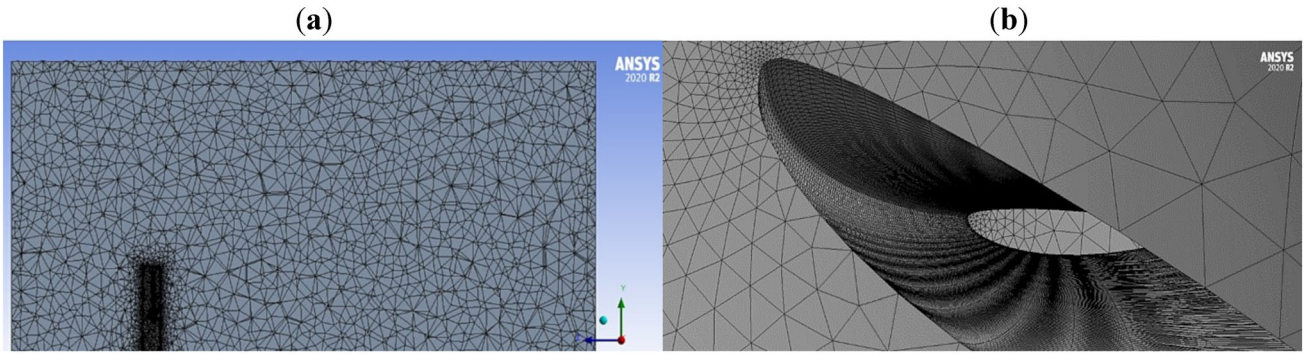
Figure 3. Computational mesh of the two fluid domains.
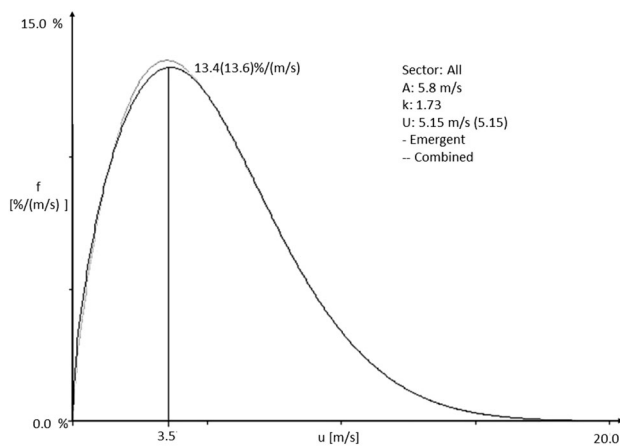
Figure 4. Weibull probability distribution of wind speed.

collected using the Global wind atlas®. The annual average wind speed was determined to be 5.15 m/s. The design wind speed was calculated as 7.25 m/s as per the IEC standard [24]. As per the WASP data, average wind speed V_{avg} = 5.15 ms^{-1} . However, the maximum probable wind speed value is 3.57 ms^{-1}.

$$V_{design} = 1.4 * V_{avg} \qquad (1)$$

3.2 Selection of airfoil

The performance of small turbines at low wind speeds is significantly influenced by the airfoil that is selected for the blade cross-section. In the case of large turbines, airfoils having a thickness greater than 25% of the chord (width of blade cross-section) are used near the root region for structural strength [10]. These airfoils exhibit poor aero-dynamic performance at low and are not preferred for small turbines. From the literature, it is found that the airfoils suitable for low applications have a thickness in the range of 7.26–16% of chord [25–27]. Since the blades of a small

turbine experience greater centrifugal load, the selected airfoil must possess sufficient thickness while exhibiting good low R_e performance. The selection of airfoil is dependent on the at which it has to operate. However, R_e is a function of relative wind speed (V_{rel}), kinematic viscosity (v), and the characteristic length i.e., the chord length (c) of the airfoil. Since the chord length is initially unknown, its value at midspan for the 1.1 m long blade was estimated to be 0.1051 m, following the guidelines provided by Manwell *et al*, for an optimum rotor with 3 blades at a tip speed ratio of 6 [17]. Similar approach was followed in the present work keeping the design tip speed ratio (λ_{design}) of 6.5 [27, 28]. Based on this assumption, the at the midspan of the blade was calculated to be 164,000 using Equations 2,3 and 4. The BEMT method is the universally accepted approach to analyse blade performance [29, 30]. In the present work BEM method is used to predict initial and modified blade performance. Table 1 provides the initial input parameters required for BEMT Approach

$$\lambda_{r_i} = \lambda_{design} * \frac{r_i}{R} \qquad (2)$$

$$V_{rel,i} = V_{design} \sqrt{1 + \lambda_{r_i}^2} \qquad (3)$$

$$R_e = \frac{V_{rel,i} * c_i}{v} \qquad (4)$$

$$c = \frac{8\pi r_i}{BC_{l,design,i}} * (1 - cos\phi) \qquad (5)$$

Table 1. Input parameters.

Parameters	Values
Power output	350 W
Freestream velocity	5.15, 7.5 and 10 m/s
Rotor radius	1.1 m
No. of sections	21
Angular velocity, ω	6.5 rad/s
No. of blades	3

where c represents the section chord length and is given by Equation 5 and v represents kinamatic viscosity of the air.

Relative wind angle Relative wind angle ϕ is calculated from Equation 6.

$$\phi = \frac{2}{3}\tan^{-1}\left(\frac{1}{\lambda_r}\right) \quad (6)$$

Section pitch angle: Section pitch angle, θ_p is calculated from the Equation 7 at each radial sections.

$$\alpha = \phi - \theta_p \quad (7)$$

The over all blade loss factor: Total blade loss factor F is calculated using the Equation 8 as given below.

$$F = F_{tip} * F_{hub} \quad (8)$$

$$F_{tip} = \frac{2}{\pi}\cos^{-1}\left[e^{\left(\frac{B(r_t - r_h)}{2rsi}\right)}\right] \quad (9)$$

$$F_{hub} = \frac{2}{\pi}\cos^{-1}\left[e^{\left(\frac{B(r - r_h)}{2r_h sin\phi}\right)}\right] \quad (10)$$

where, F_{tip} is the tip loss factor given by Equation 9 and Fhub accounts the aerodynamic losses from flow over turbine hub, which is given by Equation 10. Above steps from 1 to 5 repeated until convergence for a and a' are obtained.

Axial and angular induction factor Axial and angular induction factors are calculated from the following Equations 11 and 12.

If $\alpha < 0.4$

$$a = \left[1 + \frac{4F sin^2\phi}{\frac{cB}{2\phi r}(C_l cos\phi + C_d sin\phi)}\right]^{-1} \quad (11)$$

If $\alpha > 0.4$

$$a = \frac{18F - 20 - \sqrt[3]{C_t(50 - 36) + 12F(3F - 4)}}{36F - 50} \quad (12)$$

where C_T is the thrust coefficient which is calculated as given by Equation 13:

$$C_T = \frac{8}{9} + \left(4F - \frac{40}{9}\right)a + \left(\frac{50}{9} - 4F\right)a^2 \quad (13)$$

$$a' = \frac{1}{2}\left[-1 + \sqrt{1 + \frac{4a(1 - a)}{\lambda_r^2}}\right] \quad (14)$$

From the literature seven airfoils were shortlisted which are suitable for low application [31]. The airfoils were analyzed using QBlade® software at operational of 164,000 for range of –6° to 20°. From figure 5, it can be observed that the E216 has the highest value of but suffers from a steep decline in the value of on either side of the peak which is not favorable. Although the peak value is higher in E216,
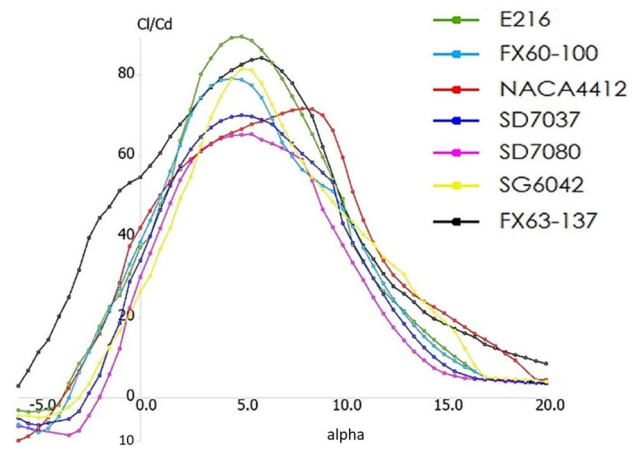
Figure 5. C_l/C_d vs α curves for low R_e airfoils at R_e=164,000 generated using QBlade®.

FX 63 looks more stable in terms of range of Angle of Attack (AoA), and (ii) E216 is a thin member and hence FX63-137 is preferred from structural stability perspective. The airfoil E216 has one of the best aerodynamic performances under low Re airfoil category. But the maximum thickness of E216 is only 10.4% of the chord. The blades of a small turbine have to withstand greater structural load. The blade is composed of only one type of airfoil throughout. Hence the selected airfoil must possess sufficient thickness while exhibiting good low Re performance. Though the airfoil E216 exhibits competitive aerodynamic performance with FX63-137 airfoil, structurally it is weak as the compared to FX63-137 airfoil where the thickness is 13.7%.

From the figure 5 it can be seen that SG6042 and FX60-100 exhibit similar behavior as E216 airfoil. The value of increases steadily with for NACA4412 airfoil and decreases suddenly after the peak with a further increase in α. However, the maximum thickness of NACA 4412 is 12% of the chord length which is favorable. The C_l/C_d vs α versus curves for SD7037, SD7080 and FX63-137 airfoils have favorable characteristic i.e., steady increase and decrease on either side of the peak with FX63-137 airfoil having the highest value of C_l/C_d. Further, the maximum thickness of FX63-137 airfoil is 13.7% of the chord, which is the highest among the seven airfoils. Selig and McGranahan [21] conducted wind tunnel tests on six airfoils including FX63-137 and analyzed their performance at R_e ranging from 100,000 to 500,000. It was found that bubble drag affected the performance of all the six airfoils at a very low R_e of 100,000. However, the drag on the FX63-137 airfoil reduced significantly as R_e increased to 150,000 and the performance improved as the R_e increased to 500,000. From the analysis performed using QBlade®, FX63-137 airfoil was selected for the blade section since it exhibits good aerodynamic characteristics and has sufficient thickness from the structural strength point of view.

3.3 Initial blade design

The blade of the wind turbine rotor was designed using BEM theory with estimated Re_{design} as 164,000 for the entire blade span. The and values required for determining the blade shape were taken from the QBlade® software output. The blade was divided into 21 sections along its span as suggested by Manwell *et al* [17]. The first airfoil section was placed at 0.121 m from the center of the rotor to accommodate the portion of the blade that attaches to the hub of the rotor. From the graph of C_l/C_d versus α at $Re_{design}, \alpha_{design}$ for each of the 21 blade sections was selected as 5.5° corresponding to C_l/C_{dmax}, where $C_{l,design}$ is the value of C_l at α_{design}.

Comparison of the experimental C_l and C_d data available in the literature [21] and the corresponding data generated by Qblade® is shown in figure 6.

It can be seen that $C_l/C_{d,max}$ occur at different values for the two datasets. Also, Qblade® slightly over-predicts the value of $C_l/C_{d,max}$ at low R_e. The C_l and D_d data generated by Qblade® is used for BEM theory-based calculations since the experimental data is not available for R_e 1,64,000. Hence this could lead to overprediction of performance by the BEM theory. However, for preliminary analysis, the aerodynamic data available in Qblade® can be used when wind tunnel test data isn't available at the desired R_e. QBlade under predicts for low AOA and over predicts for higher AOA [32]. The observed variation in the present study is due to the large number of points (160 points) considered in XFOIL(QBlade). Further, the distance between the points should be evenly spaced over the airfoil to use Trapezoidal rule for integration of C_p during C_l calculation [33]. But on the airfoil model fabricated for experiment, usually a greater number of points are provided at leading edge compared to trailing edge. As there is no literature which reported the experimental data for airfoil performance at $R_e = 1.64 * 10^5$ and QBlade is considered
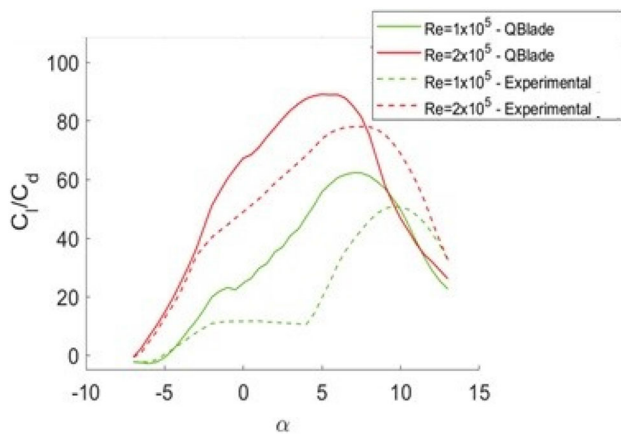
Figure 6. C_l/C_d vs α curves for FX63-137 airfoil obtained from Qblade® and Experimental data of Selig and McGranahan [21].

as reference. The c and θ_p distributions obtained are shown in figure 7(a and b).

3.4 Performance prediction of initial blade design

The power coefficient (C_p) is the measure of performance of a wind turbine rotor. It is the ratio of power extracted by the rotor to the power available in the wind. However, C_p majorly depends on the tip speed ratio (λ) of the rotor which is the ratio of rotational velocity of the rotor tip to the wind speed. The formula for tip speed ratio and power coefficient are given in Equations 15,16.

$$\lambda = \frac{R\Omega}{V} \tag{15}$$

$$C_p = \frac{8}{\lambda^2}\int_{\lambda_r}^{\lambda} F\sin^2\phi(\cos\phi - \lambda\sin\phi)$$
$$(\sin\phi + \lambda_r\cos\phi)\left[1 - \frac{C_d}{C_l}\cot\phi\right]^2 \lambda_r d\lambda_r \tag{16}$$

where P_{rotor} is the rotor power, ρ is the air density, R is radius of swept area. The plot of C_p versus λ is termed as the performance curve of a wind turbine and using these performance curves plotted at different wind speeds, one can determine the power extracted by the rotor for any combination of rotor and wind speeds. The performance curve also provides instant information about the $C_{p,max}$ and the corresponding λ_{opt} for the designed rotor. Figure 8 shows the performance curves for the initial blade design at three different wind speeds obtained from BEM theory based MATLAB® program [10].

The MATLAB® program developed by Wood [10] accounts for the axial, angular induction factors and Prandtl's tip loss factor. The C_p and C_d values of the FX63-137 airfoil required for the MATLAB® program are taken from the Qblade® software. A theoretical C_{pmax} of 0.47 is obtained at λ_{opt} of 6.45 for the design wind speed of 7.25 m/s which is not significantly different for 10 m/s.

3.5 Optimization of blade design by linearization of chord distribution and section pitch angle

In the present work, four different combinations of chord length and section pitch angle distribution were chosen in the process of linearization as shown in figure 9.

The Chord distribution of the 1st combination is obtained by drawing a straight line through the chord length values at the 1st and 21st sections of the initial blade shape. This is to ensure that the chord length of the optimized blade is not lesser than that of the initial blade shape. Section pitch angle distribution of the 1st combination is obtained by drawing a straight line through the pitch angles at the 3rd and 21st sections of the initial blade shape. The other three
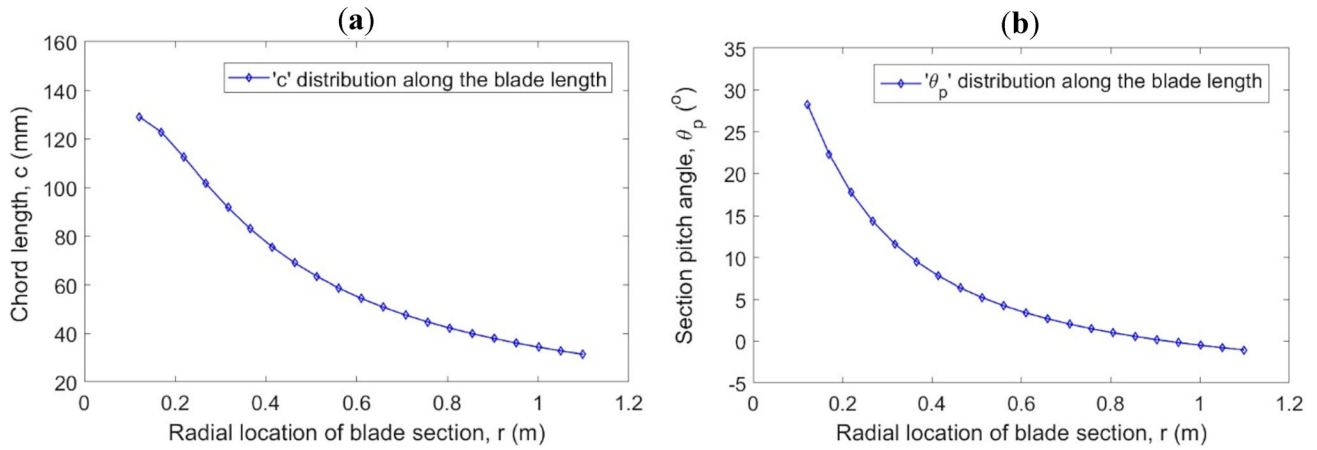
Figure 7. (**a**) Chord length distribution along the blade span. (**b**) Section pitch angle distribution.
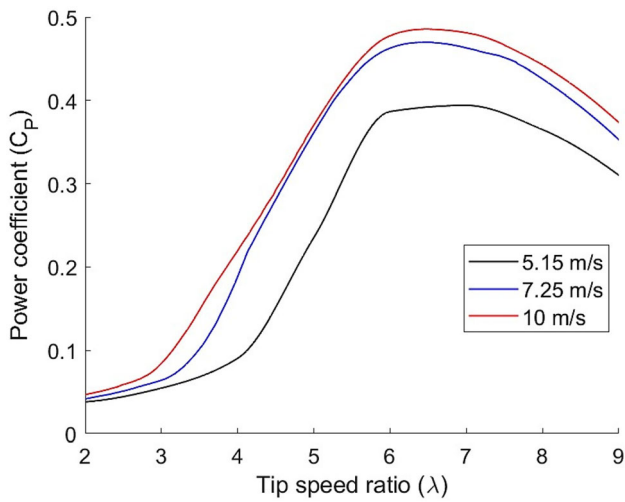
Figure 8. Performance curve of initial blade design at different wind speeds.

combinations are weighted averages between the initial blade shape and the 1*st* combination. The weightages used for obtaining 2*nd*, 3*rd* and 4*th* combinations are shown in table 2. The performance curves for different combinations obtained from the MATLAB® programs is shown in figure 10. It can be seen that that all four combinations have better C_p when compared to the initial blade shape for λ in the range of 4 to 6. One can observe that the 1*st* combination with a linear distribution of section pitch angle has the widest performance curve at all the wind speeds considered. However, figure 10(a) shows that C_p for the 1*st* combination is significantly lesser at a wind speed of 5.15 m/s when compared to other three combinations.

From the analysis of performance curves shown in figure 10, the 4*th* combination is selected as the optimum blade shape since it has better C_p when compared to the initial blade shape for all values of λ less than 6.5. Comparison of $C_{p,max}$ for initial and combination 4 blade shape
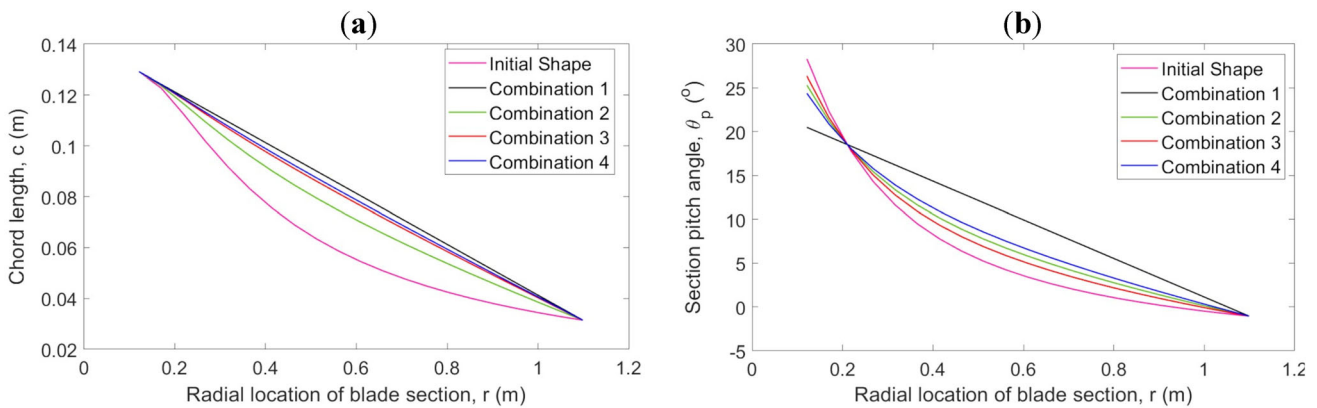

Figure 9. (**a**) Chord length and (**b**) Section pitch angle distribution for initial blade shape and different combinations.

**Table 2.** Linearization method for different combinations.

Combination	Chord distribution weightage (%)		Section pitch angle distribution weightage (%)	
	Initial blade shape	Combination 1	Initial blade shape	Combination 1
2	40	60	60	40
3	15	85	75	25
4	10	90	50	50
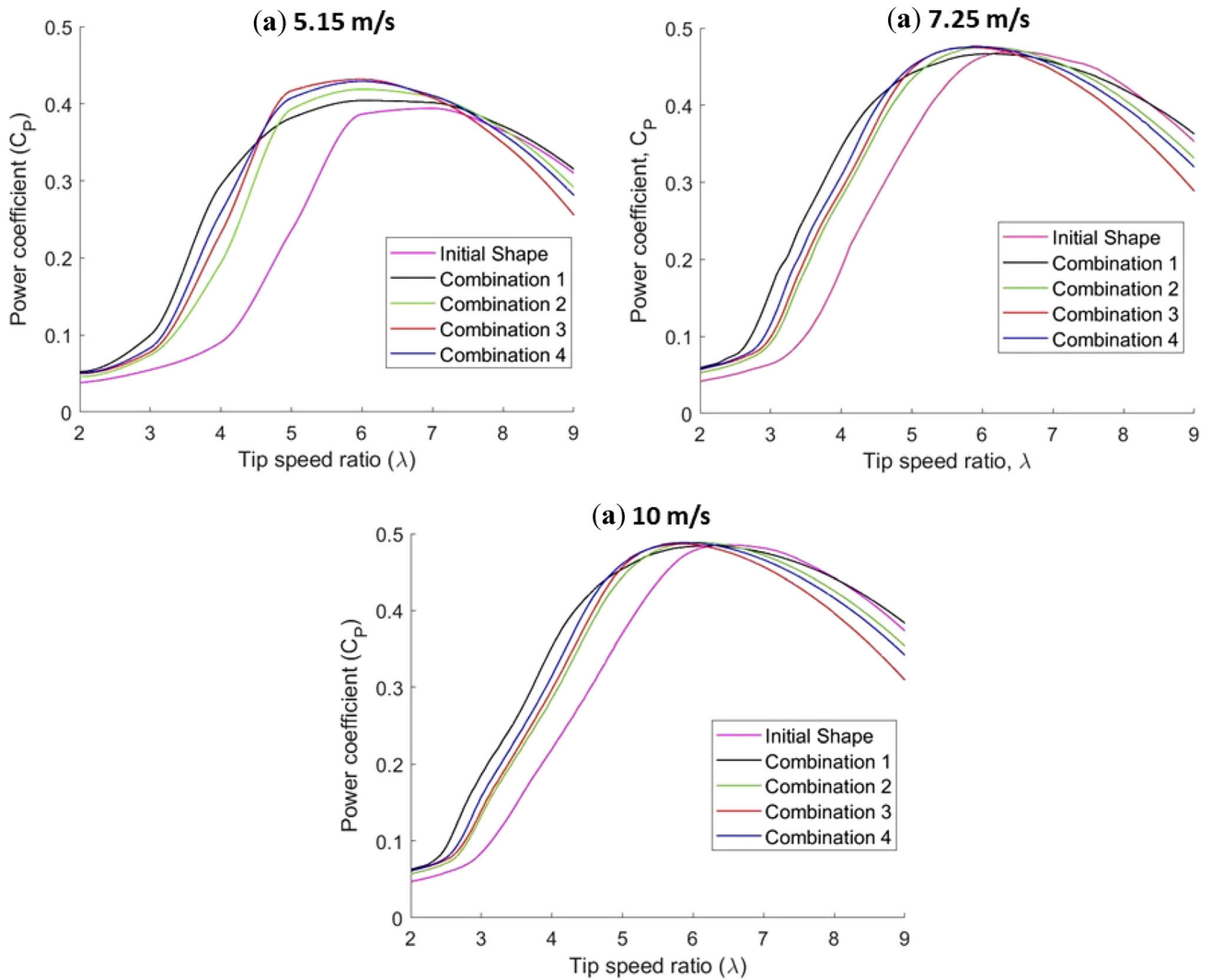
Figure 10. Performance curves of four combinations at three different wind speeds.

Table 3. Comparison of $C_{p,max}$ for initial and combination 4 blade shapes.

Wind speed (m/s)	$C_{p,max}$ at corresponding λ_{opt}		Improvement (%)
	Initial blade shape	Combination 4	
5.15	0.396 at 7.1	0.429 at 6.31	8.33
7.25	0.469 at 6.45	0.476 at 5.89	1.49
10	0.485 at 6.45	0.488 at 5.89	0.62
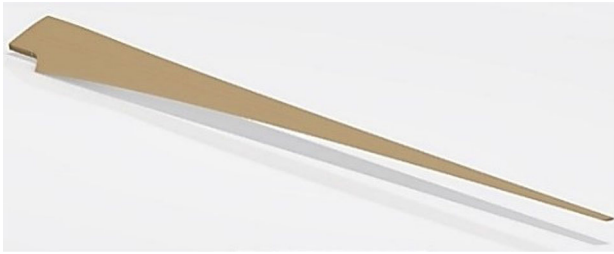
**Figure 11.** Optimized blade shape derived from combination 4.

is shown in table 3, it is evident that the improvement in C_p for the optimized blade is significant at a wind speed of 5.15 m/s.

This may be attributed to the increase in the chord length at the middle portion of the optimized blade. It must be noted that the optimized blade shape has $C_{p,max}$ at a lesser value of λ_{opt} when compared to the initial blade. This might benefit the blade design from the structural strength point of view. Because the turbine can generate greater power at lower rotor speeds thereby reducing the centrifugal load acting on the blade. Hence, the combination 4 is used for subsequent numerical study which is explained in section 3.6.

3.6 *CFD simulation*

3.6.1 *Validation* Using CFD simulation, one can also determine the pressure exerted by the flow over the blade that can be used further in flow visualization studies in future work. Furthermore, CFD simulation aid the calculation of power and torque developed by the rotor.
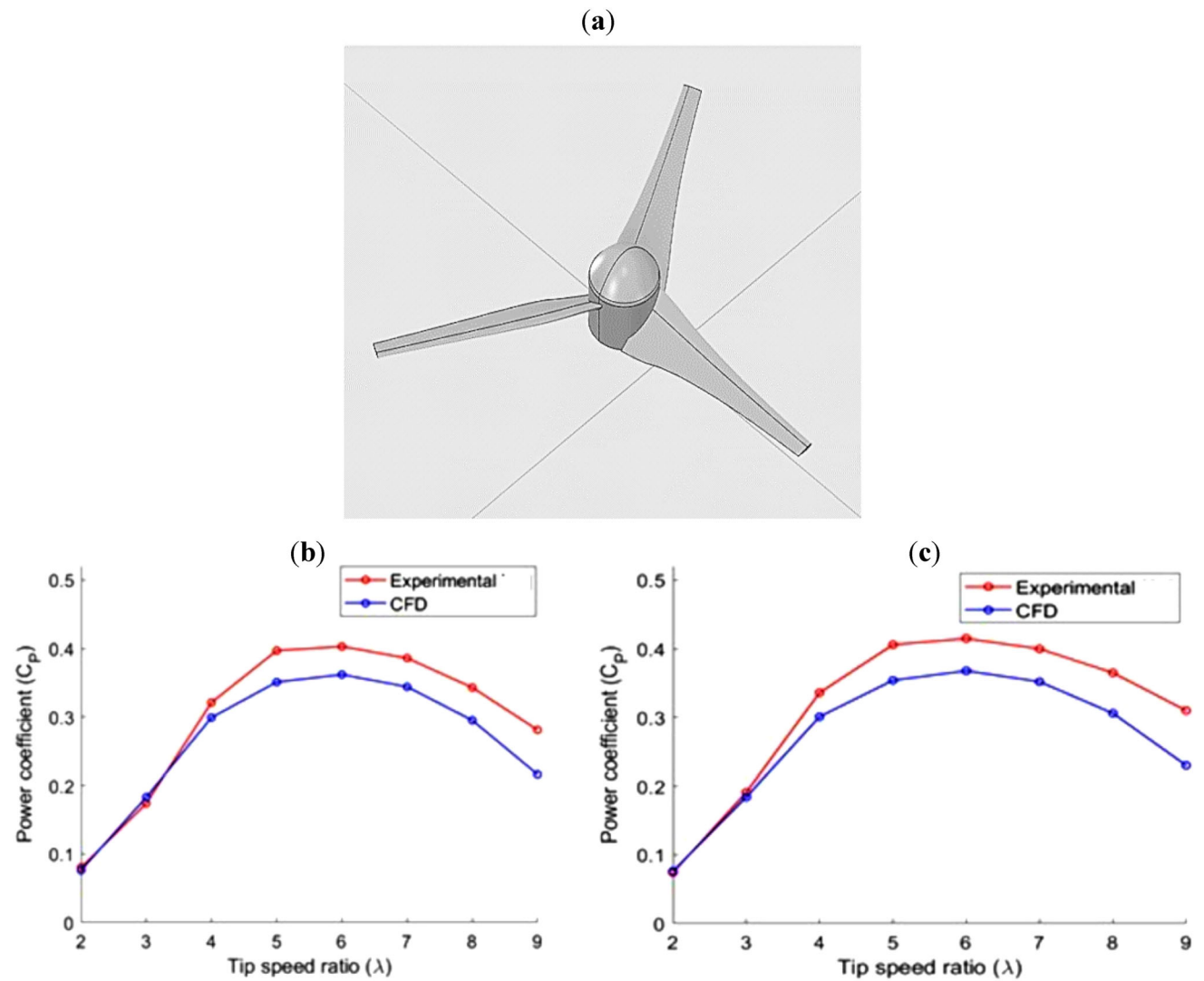
Figure 12. (**a**) 1.3 m diameter rotor made of SD8000 airfoil [22]. Performance curve Experimental data [22] vs CFD from present work at (**b**) 6 m/s, (**c**) 8 m/s.
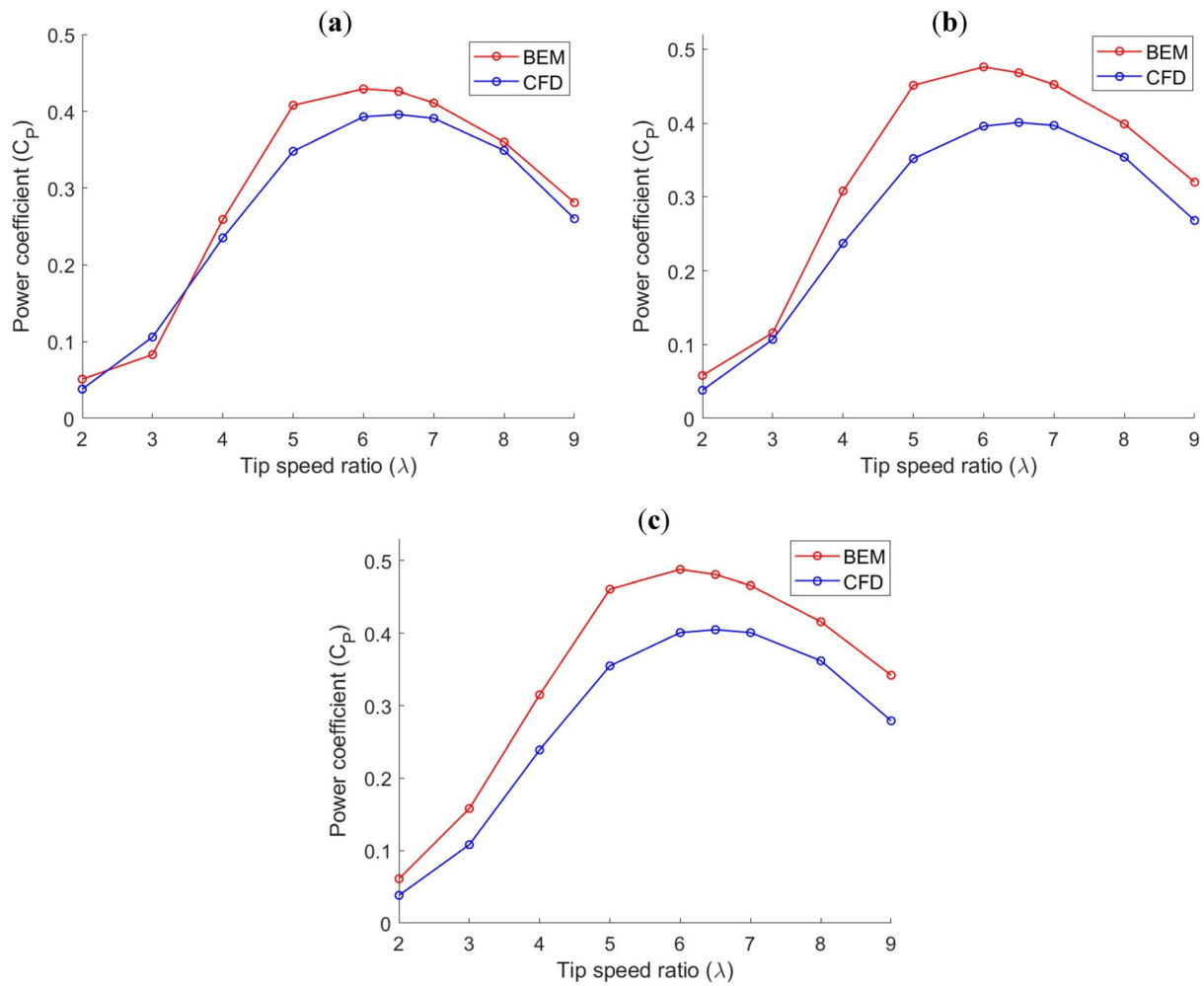
Figure 13. Performance curves for the optimized blade obtained from BEM theory and CFD simulation (**a**) at 5.15 m/s, (**b**) at 7.25 m/s, (**c**) at 10 m/s.

Table 4. Comparison of $C_{p,max}$ for initial and combination 4 blade shapes.

$C_{p,max}$ at corresponding λ_{opt}			
Wind speed (m/s)	CFD simulation	BEM theory	Variation (%)
5.15	0.396 at 6.5	0.429 at 6.31	8.32
7.25	0.405 at 6.5	0.488 at 5.89	18.84
10	0.401 at 6.5	0.476 at 5.89	20.50

Combination 4 is the optimized blade shape that was later modelled using 3D Experience® platform and is shown in figure 11.

The CFD simulation methodology incorporated in this study was validated using experimental studies from the literature as shown in figure 12(a). A 1.3 m diameter HAWT having an experimentally determined performance curve was simulated using the MRF approach in ANSYS Fluent®. A SD8000 airfoil was used for the cross-section of the HAWT blade. Boundary conditions were maintained similar to the experimental set-up of Chen *et al*

Dimensions of the blade and the experimentally determined performance curve are available in the literature. CFD simulation is carried out at different λ for wind speed of 6 ms^{-1} [34]. The performance curves obtained from the simulation and experiment are shown in figure 12(b and c). The observation is valid as the C_p was calculated for 6 and 8 m/s. Moreover, this was a validation study and the maximum variation between the results of experiments in literature and CFD simulation of the present work was found to be 9.53 and 11.15% at 6 and 8 m/s respectively.

Shu *et al* [35] performed steady-state simulations using MRF approach to estimate the performance of clean blades as well as blades with icing on their surface. It was observed that the results of the CFD simulation were in good agreement with the experiments for clean blades. However, the performance of the blades with icing was overpredicted by the CFD simulation. Zhang *et al* [36] studied the effect of gurney flaps on the performance of a 2 m diameter rotor with two blades using MRF approach. A maximum error of 14.1% was observed between the results of experiments and CFD simulations. The CFD simulation uses the MRF approach which is a steady-state approximation of a transient flow phenomenon. This could be the possible reason for the variation in the results of simulations and experiments. However, CFD simulation predicts C_{pmax} at λ_{opt} of 6 which agrees with the experimental results. Therefore, MRF approach can be used to perform CFD simulations even with limited computational resources.

3.6.2 *CFD results* Steady-state simulations were carried out using ANSYS FLUENT® to determine the torque on the rotor at different wind speeds and λ. Using the value of torque obtained from CFD simulation, the power and power coefficient are calculated using Equation 10 and Equation 9 respectively. The performance curves obtained from the CFD simulation and from the BEM theory are shown in figure 13 and table 4.

It can also be observed that the performance curves obtained from CFD simulation and BEM theory are in good agreement at a wind speed of 5.15 m/s. Further, at wind speed of 7.25 m/s and tip speed ratio of around 6.5, the power coefficient is found to be the highest. However, the variation in the results is relatively larger at wind speeds of 7.25 and 10 m/s. The variation in the C_{pmax} may be attributed to the discrepancies in the C_l and C_d data used for BEM theory-based predictions, as shown in figure 6, as well as the steady-state approximation of the MRF approach.

4. Conclusions

In the present work, a horizontal axis wind turbine (HAWT) blade was designed to harness energy from low wind velocity (between 5 and 10 m/s). The 1.1 m long blade was initially designed using the BEM theory. The initial design was optimized by linearizing the chord and section pitch angle distribution. The objective of optimization was to achieve wider and better aerodynamic performance curves at different operational wind speeds. The following are the conclusions from the present study:

(1) It was found that the optimized blade had an improvement of 8.33% in power coefficient (C_p), at 5.15 m/s when compared to the initial design.

(2) From the CFD simulation it was found that the optimized blade, made of FX63-137 airfoil, was capable of obtaining highest value of C_p at wind speed of 7.25 m/s at tip speed ratio of 6.5.

(3) The average variation in C_p predicted by CFD simulation and BEM theory, was found to be 5.91% at wind speed of 5.15 m/s and 21.72% at 10 m/s. It was found that BEM theory slightly overpredicts the performance of the turbine blade.

(4) The multiple reference frame (MRF) approach used for CFD simulation was validated using the experimental data from the literature. The average variation between the results of CFD simulation and the experimental data in the literature was found to be 9.53% at 6 m/s and 11.15% at 8 m/s.

Current work is focussed on combination approach of blade design starting from BEMT. Future work consists of identifying the Laminar separation bubble (LSB) and reducing the LSB by boundary layer trips, analysis on structural stability of the blade followed by fabrication and testing in the wind tunnel lab to corroborate with the simulation studies [37].

Abbreviations

BEM	Blade element momentum
BLT	Boundary layer trip
CFD	Computational fluid dynamics
HAWT	Horizontal axis wind turbine
IEC	International Electrotechnical Commission
LSB	Laminar separation bubble
MRF	Multiple reference frame
SWT	Small wind turbine
VAWT	Vertical axis wind turbine

Greek symbols

α	Angle of attack, °
λ	Tip speed ratio
ω	Angular velocity of the turbine rotor, rad/s
ϕ	Angle of relative wind, °
ρ	Density of air, kg/m3
θ_p	Section pitch angle, °
v	Kinematic viscosity, m2/s

List of symbols

C_d	Coefficient of drag
C_l	Lift coefficient
C_p	Power coefficient
P_{rotor}	Power captured by the turbine rotor, W
R_e	Reynolds number
V_{avg}	Average wind speed, m/s
V_{design}	Design wind speed, m/s
V_{rel}	Relative wind speed, m/s
a	Axial induction factor

a'	Angular induction factor
B	Number of blades
c	Chord length, m
R	Radius of the turbine rotor, m
r	Radial location of the blade section, m
T	Torque acting on the turbine rotor, Nm
V	Wind speed, m/s

Subscripts

design	Design condition
h	Hub
i	Blade section designation
max	Maximum value
opt	Optimum value
t	Tip

Acknowledgements

References

[1] Francis Muyiwa F, Ajayi Oluseyi O and Ojo Joseph O 2021 Development of a novel airfoil for low wind speed vertical axis wind turbine using QBlade simulation tool. *Fuel Commun.* 9: 100028

[2] Siram Ojing, Saha Ujjwal K and Sahoo Niranjan 2022 Blade design considerations of small wind turbines: From classical to emerging bio-inspired profiles/shapes. *J. Renew. Sustain. Energy*, 14(4)

[3] Maegaard P, Krenz A, Adsal K A, Pitteloud J-D, Gsänger S and Ogg F 2016 Catalogue of small wind turbines (under 50 kw). report. Technical report, Nordic Folk center for Renewable Energy, Denmark

[4] Karthikeyan N, Kalidasa M K, Arun K S and Rajakumar S 2015 Review of aerodynamic developments on small horizontal axis wind turbine blade. *Renew. Sustain. Energy Rev.* 42: 801–822

[5] Krishnanunni AR, Datta N, Chambhare HS and Swaroop D 2020 Basic design and blade structural analysis of a small horizontal-axis wind turbine for low wind speeds. In: *ASME Power Conference*, vol. 83747, pp. V001T08A011. American Society of Mechanical Engineers

[6] Hani M, Wael A-K and Waqar K 2019 Small wind turbine blade design and optimization. *Symmetry* 12(1): 18

[7] Singh Ronit K, Rafiuddin A M, Asid Z M and Young-Ho L 2012 Design of a low reynolds number airfoil for small horizontal axis wind turbines. *Renew. Energy* 42: 66–76

[8] Song Q and Lubitz W D 2014 Design and testing of a new small wind turbine blade. *J. Solar Energy Eng.* 136(3): 034502

[9] Refan M and Hangan H 2012 Aerodynamic performance of a small horizontal axis wind turbine

[10] Wood D 2011 Small wind turbines. In: *Advances in wind energy conversion technology*, pp. 195–211. Springer

[11] Abhishiktha T, Kishore V R, Kumar S D, Indraja V and Hari K V 2016 A review on small scale wind turbines. *Renew. Sustain. Energy Rev.* 56: 1351–1371

[12] Clausen P D, Reynal F and Wood D H 2013 *Advances in wind turbine blade design and materials: 13. Design, manufacture and testing of small wind turbine blades.* Elsevier Inc. Chapters

[13] Horizon G-B 2012 Low speed wind turbine design. IntechOpen, London

[14] Ahmad S, Mojtaba M and Mahdi M Z 2014 Aerodynamic design and economical evaluation of site specific horizontal axis wind turbine (HAWT). *Energy Equip. Syst.* 2(1): 43–56

[15] Siram O and Sahoo N 2022 Performance assessment of straight and linearly tapered rotors through wind tunnel investigation for off-grid applications. *Wind Eng.* 46(4): 1291–1310

[16] Saeed R, Abolfazl P, Abbas K S A and Raza K S M 2020 Performance analysis of a small horizontal axis wind turbine under the use of linear/nonlinear distributions for the chord and twist angle. *Energy Sustain. Dev.* 58: 42–49

[17] Manwell James F, McGowan Jon G and Rogers Anthony L 2010 Wind energy explained: theory, design and application. John Wiley & Sons

[18] Tony B, Nick J, David S and Ervin B 2011 Wind energy handbook. John Wiley & Sons

[19] Wood David 2011 Small wind turbines. In: *Advances in wind energy conversion technology*, pp. 195–211. Springer

[20] Bakırcı M and Yılmaz S 2018 Theoretical and computational investigations of the optimal tip-speed ratio of horizontal-axis wind turbines. *Eng. Sci. Technol. Int. J.* 21(6): 1128–1142

[21] Selig Michael S and McGranahan Bryan D 2004 Wind tunnel aerodynamic tests of six airfoils for use on small wind turbines. *J. Sol. Energy Eng.* 126(4): 986–1001

[22] Bai C-J and Wang W-C 2016 Review of computational and experimental approaches to analysis of aerodynamic performance in horizontal-axis wind turbines (HAWTS). *Renew. Sustain. Energy Rev.* 63: 506–519

[23] Tang X 2012 *Aerodynamic design and analysis of small horizontal axis wind turbine blades.* PhD thesis, University of Central Lancashire

[24] IEC 61400.2-2013 2013 Wind turbines part 2. design requirements for small wind turbines

[25] Giguere P and Selig M S 1997 Low reynolds number airfoils for small horizontal axis wind turbines. *Wind Eng.*, pp. 367–380

[26] Giguere P and Selig M S 1998 New airfoils for small horizontal axis wind turbines

[27] Singh Ronit K and Rafiuddin A M 2013 Blade design and performance testing of a small wind turbine rotor for low wind speed applications. *Renew. Energy* 50: 812–819

[28] Bai C J, Hsiao F B, Li M H, Huang G Y and Chen Y J 2013 Design of 10 kw horizontal-axis wind turbine (HAWT) blade and aerodynamic investigation using numerical simulation. *Proced. Eng.* 67: 279–287

[29] Cabanillas S V 2013 Blade performance analysis and design improvement of a small wind turbine for rural areas. Master's thesis, Universitat Politècnica de Catalunya

[30] Song Q 2012 *Design, fabrication, and testing of a new small wind turbine blade*. PhD thesis, University of Guelph

[31] Miley S J 1982 Catalog of low-reynolds-number airfoil data for wind-turbine applications. Technical report, Rockwell International Corp., Golden, CO (USA). Rocky Flats Plant; Texas A

[32] Chen W and Bernal L 2008 Design and performance of low reynolds number airfoils for solar-powered flight. In: *46th AIAA aerospace sciences meeting and exhibit*, pp. 316

[33] Drela M 1989 Xfoil: An analysis and design system for low reynolds number airfoils. In: *Low Reynolds Number Aerodynamics: Proceedings of the Conference Notre Dame, Indiana, USA*, pp. 1–12. Springer

[34] Yu-Jen C, Guo-Yuan H, Shiah Y C and Yi-Lun T 2020 Performance prediction for small horizontal axis wind turbine (HAWT) by integrated theory and experimental verifications. *Int. J. Precis. Eng. Manuf. -Green Technol.* 7: 131–140

[35] Lichun S, Li Hantao H, Qin J X, Gang Q, Gaohui H and Yanqing L 2018 3d numerical simulation of aerodynamic performance of iced contaminated wind turbine rotors. *Cold Reg. Sci. Technol.* 148: 50–62

[36] Ye Z, Varun R, Zohaib S, Xiaofang W, Gerard S and Carlos F 2019 Effects of root gurney flaps on the aerodynamic performance of a horizontal axis wind turbine. *Energy* 187: 115955

[37] Lhoussaine T, Yassine K, Farid A and Anas B 2021 Structural design and analysis of a small wind turbine blade using Simple Load Model, FAST-Mlife codes, and ANSYS nCode DesignLife. *Wind Eng.* 45(2): 213–230